NASA TN D-1951

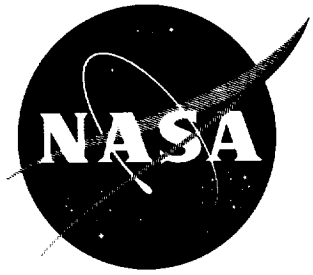

TECHNICAL NOTE

D-1951

CONTROL OF A LARGE LAUNCH VEHICLE WITH LIMITED THRUST VECTORING IN THE PRESENCE OF WINDS

By Dennis F. Collins, Jr., and Homer G. Morgan

Langley Research Center
Langley Station, Hampton, Va.

NATIONAL AERONAUTICS AND SPACE ADMINISTRATION
WASHINGTON August 1963

NATIONAL AERONAUTICS AND SPACE ADMINISTRATION

TECHNICAL NOTE D-1951

CONTROL OF A LARGE LAUNCH VEHICLE WITH LIMITED THRUST VECTORING IN THE PRESENCE OF WINDS

By Dennis F. Collins, Jr., and Homer G. Morgan

SUMMARY

An investigation has been made to determine the controllability of a large launch vehicle with limited thrust vectoring which permits the aerodynamic upsetting moment due to winds to exceed temporarily the control moment. The analysis was restricted to the pitch plane and included time-varying coefficients and longitudinal translation, normal translation, rigid-body pitch, and thrust-vectoring angle as degrees of freedom. A simple closed-loop control system utilizing attitude and attitude-rate feedback was employed. The vehicle was flown vertically through 1-percent and 5-percent synthetic wind profiles on an analog computer.

The results are presented as time histories of attitude angle and angle of attack and as plots of attitude angle against limit thrust-vectoring angle with the attitude gain and attitude-rate gain as parameters. It is concluded that if the limit thrust-vector angle is near the thrust-vector angle required with no limit, the vehicle is able to recover from the temporary instability resulting from large wind disturbances. This results in an additional safety factor for a control system that has been designed with adequate thrust vectoring to maintain control for specified wind and payload conditions. It is also shown herein that for a given vehicle flying through a given wind profile, there is some minimum value of limit thrust-vector rotation angle, independent of control-system gains, below which the vehicle is always divergent.

INTRODUCTION

The conventional method of control of large launch vehicles is by thrust vectoring. Disturbances are sensed by an autopilot which commands a rotation of the rocket engine's thrust vector to create a restoring moment on the launch vehicle. The amount of thrust-vector rotation required is determined by the magnitude of the disturbing forces. The largest disturbances are usually aerodynamic and result from winds in the maximum-dynamic-pressure portion of the launch trajectory. For design purposes, a synthetic wind profile, such as that of reference 1, is normally used to determine the maximum expected disturbances and, thus, the maximum anticipated thrust-vector rotation angle.

It is the purpose of this paper to investigate the behavior of a large launch vehicle (from the viewpoint of controllability) when the thrust-vector rotation angle is limited so that the aerodynamic upsetting moment exceeds the control moment and permits a temporarily unstable condition to exist. Conditions are favorable for this temporary instability to exist in the neighborhood of the characteristic wind-shear reversal which occurs near an altitude of 35,000 feet on most wind profiles. However, the vehicle passes through this wind "spike" in a very short time - about 5 seconds - and control may be recovered before the vehicle has time to diverge. Control recovery would be assisted by the rapidly decreasing dynamic pressure after the vehicle passes through the wind-shear reversal.

In this paper, a study is made of the ability of a launch vehicle of the Nova class to fly through wind-shear reversals while temporarily unstable. The vehicle is considered to be a rigid body flying through synthetic wind profiles from reference 1. The limit on the thrust-vector rotation angle is similar to mechanical stops on a gimbaled engine. The ability of the vehicle to recover from the unstable conditions is examined as a function of the maximum thrust-vector angle permitted.

SYMBOLS

$A(x)$	cross-sectional-area distribution, sq ft
A_e	area of exhaust-exit face, sq ft
A_o	reference area (base of vehicle), sq ft
C_{m_α}	pitching-moment coefficient per unit angle of attack, 1/radian
$C_{m_{\dot{\theta}}}$	pitching-moment coefficient per unit pitch velocity, 1/radian
C_{N_α}	normal-force coefficient per unit angle of attack, 1/radian
$C_{N_{\dot{\theta}}}$	normal-force coefficient per unit pitch velocity, 1/radian
C_X	axial-force coefficient
F	thrust, lb
F_A	aerodynamic force, lb
F_g	gravity force, lb
F_P	propulsion force, lb

F_X, F_Y	external force components in axial and lateral directions, lb
g	acceleration due to gravity, ft/sec^2
h	altitude, ft
h_o	initial altitude, ft
I	instantaneous mass moment of inertia, $lb\text{-}sec^2\text{-}ft$
I_{sp}	specific impulse, sec
$\bar{i}$	unit vector in the axial direction
$\bar{j}$	unit vector in the lateral direction
K_1	attitude gain
K_2	attitude-rate gain, sec
$L(x,t)$	time-dependent normal-force distribution, lb/ft
l_B	length of vehicle forward of thrust-vector rotation point, ft
l_E	length of engine, ft
M	moment of external forces about the vehicle center of gravity, lb-ft
M_A	aerodynamic moment about the vehicle center of gravity, lb-ft
M_P	moment of propulsion forces about the vehicle center of gravity, lb-ft
m	instantaneous mass, $lb\text{-}sec^2/ft$
$m_B(\eta)$	body mass distribution, $lb\text{-}sec^2/ft^2$
$m_E(\xi)$	engine mass distribution, $lb\text{-}sec^2/ft^2$
m_o	initial vehicle mass, $lb\text{-}sec^2/ft$
$\bar{n}$	unit vector normal to exhaust-exit face
q	dynamic pressure, $\frac{1}{2}\rho V^2$, lb/sq ft
$\bar{r}$	vector from vehicle center of gravity to exhaust-exit face, ft
S_E	gimbaled-engine static unbalance, $lb\text{-}sec^2$

T	kinetic energy, ft-lb
t	time, sec
t_o	initial time, sec
V	magnitude of vehicle velocity relative to wind, ft/sec
$\bar{V}_B$	velocity vector of a point on the vehicle, ft/sec
$\bar{V}_E$	velocity vector of a point on the engine, ft/sec
$\bar{V}_e$	inertial velocity of exhaust, ft/sec
$\bar{V}_{e,cg}$	velocity of exhaust relative to vehicle center of gravity, ft/sec
$\bar{V}_{e,E}$	velocity of exhaust relative to a point fixed on engine, ft/sec
$V_{e,n}$	magnitude of exhaust exit velocity relative to nozzle, ft/sec
V_i	magnitude of vehicle inertial velocity, ft/sec
V_w	horizontal atmospheric wind velocity, ft/sec
V_X, V_Y	axial and lateral components of vehicle center-of-gravity velocity, ft/sec
$w(x,t)$	local time-dependent downwash velocity, ft/sec
x	body coordinate measured from thrust-vector rotation point, ft
x_{cg}	center-of-gravity location, measured from thrust-vector rotation point, ft
x_e	distance from thrust-vector rotation point to exhaust-exit face, ft
α	angle of attack due to inertial motion, radians unless otherwise specified
α_w	angle of attack due to atmospheric wind, radians unless otherwise specified
β	ratio of attitude gain to nominal attitude gain
Γ	ratio of attitude-rate gain to nominal attitude-rate gain
γ	flight-path angle, radians

δ thrust-vector rotation angle, radians unless otherwise specified

δ_c command thrust-vector rotation angle, radians unless otherwise specified

δ_{lim} limit thrust-vector rotation angle, radians unless otherwise specified

η dummy variable of integration, ft

θ vehicle attitude angle, radians unless otherwise specified

μ rate at which mass is expelled from vehicle, lb-sec/ft

ξ dummy variable of integration, ft

ρ atmospheric density, slugs/cu ft

ρ_e exhaust density, slugs/cu ft

τ thrust-vectoring time lag, sec

Subscripts:

X axial direction

Y lateral direction

A dot over a symbol denotes differentiation with respect to time.

A bar over a symbol denotes a vector.

ANALYSIS

The equations of motion for this study were derived from Lagrange's equations modified for use in a rotating coordinate system as discussed in reference 2. The coordinate system is illustrated in figure 1. This method requires that the kinetic energy T be derived and operated on by the following set of equations to obtain the differential equations for the forces and moment:

$$\frac{d}{dt}\left(\frac{\partial T}{\partial V_X}\right) - \dot{\theta}\left(\frac{\partial T}{\partial V_Y}\right) = \Sigma F_X \tag{1a}$$

$$\frac{d}{dt}\left(\frac{\partial T}{\partial V_Y}\right) + \dot{\theta}\left(\frac{\partial T}{\partial V_X}\right) = \Sigma F_Y \tag{1b}$$

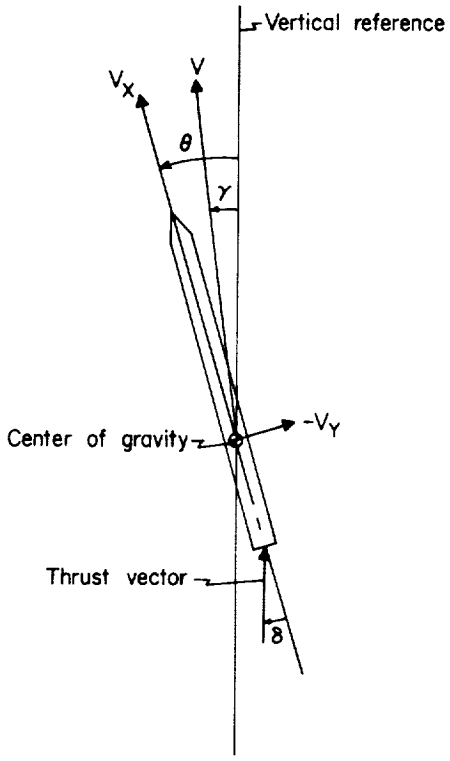

Figure 1.- Coordinate system.

$$\frac{d}{dt}\left(\frac{\partial T}{\partial \dot{\theta}}\right) + V_X\left(\frac{\partial T}{\partial V_Y}\right) - V_Y\left(\frac{\partial T}{\partial V_X}\right) = \Sigma M \qquad (1c)$$

where V_X and V_Y are the axial and lateral components of the center-of-gravity velocity, $\dot{\theta}$ is the pitch velocity about the center of gravity, F_X and F_Y are the external force components in the axial and lateral directions, and M is the moment of the external forces about the center of gravity.

Kinetic Energy

The total kinetic energy of a launch vehicle with a gimbaled engine may be written as the kinetic energy of the vehicle less the engine plus the kinetic energy of the engine:

$$T = \frac{1}{2}\int_{l_B} m_B(\eta)\bar{V}_B\cdot\bar{V}_B \, d\eta + \frac{1}{2}\int_{l_E} m_E(\xi)\bar{V}_E\cdot\bar{V}_E \, d\xi \qquad (2)$$

where the subscripts B and E refer to the body (vehicle less engine) and the engine, respectively, $\bar{V}_B$ and $\bar{V}_E$ are the velocities of points on the body and engine, and m_B and m_E are the respective mass distributions. The velocity vector $\bar{V}_B$ is given by

$$\bar{V}_B = \bar{i}V_X + \bar{j}\left[V_Y + \dot{\theta}\left(x - x_{cg}\right)\right] \qquad 3(a)$$

and the velocity of a point on the engine is given by

$$\bar{V}_E = \bar{i}\left[V_X - (\dot{\theta} - \dot{\delta})d(\xi)\sin\delta\right] + \bar{j}\left[V_Y - \dot{\theta}x_{cg} - (\dot{\theta} - \dot{\delta})d(\xi)\cos\delta\right] \qquad 3(b)$$

Forces and Moment

The forces and moment are made up of contributions from aerodynamic forces, propulsion forces, and gravity forces, and may be expressed in the following form:

$$\Sigma F_X = F_{A,X} + F_{P,X} + F_{g,X} \qquad (4)$$

$$\Sigma F_Y = F_{A,Y} + F_{P,Y} + F_{g,Y} \tag{5}$$

$$\Sigma M = M_A + M_P \tag{6}$$

where the subscripts A, P, and g refer to aerodynamic, propulsion, and gravity, respectively.

Aerodynamic forces.- Slender-body theory, as described in reference 3, was used for this study. The normal-force distribution is given by

$$L(x,t) = -\rho\left(V\frac{\partial}{\partial x} - \frac{\partial}{\partial t}\right)\left[A(x)w(x,t)\right] \tag{7}$$

The cross-sectional-area distributions $A(x)$ were obtained from figure 2, and all cross sections of the vehicle, including those through the fins, were assumed to be circular. The local applied downwash $w(x,t)$ is given by

$$w(x,t) = V\left[(\theta - \gamma) + \alpha_w\right] - \dot{\theta}\left(x - x_{cg}\right) \tag{8}$$

The wind-induced angle of attack α_w is approximated by the following equation:

$$\alpha_w = \frac{V_w}{V}\cos\gamma \tag{9}$$

where V_w is the horizontal wind velocity and V is the vehicle velocity relative to the wind. These velocities are defined in the following manner:

$$V^2 = V_i^2 + V_w^2 - 2V_iV_w\sin\gamma \tag{10}$$

and

$$V_i^2 = V_X^2 + V_Y^2 \tag{11}$$

The aerodynamic force acting normal to the vehicle is

$$F_{A,Y} = \int_{l_B} L(x,t)dx \tag{12}$$

The aerodynamic moment about the center of gravity is

$$M_A = \int_{l_B} \left(x - x_{cg}\right) L(x,t)\,dx \tag{13}$$

The axial aerodynamic force is

$$F_{A,X} = \frac{1}{2}\rho V^2 C_X A_o \tag{14}$$

where C_X is the axial-force coefficient and A_o is the cross-sectional area of the vehicle base.

Propulsion forces and moment.- Vector equations for the propulsion forces $\bar{F}_P$ and moment $\bar{M}_P$ including the effects of engine motion can be obtained from reference 4 and are given by

$$\bar{F}_P = - \int_{A_e} \rho_e \bar{V}_e \left(V_{e,E} \cdot \bar{n}\, dA_e\right) \tag{15}$$

$$\bar{M}_P = - \int_{A_e} \bar{r} \times \rho_e \bar{V}_{e,cg} \left(\bar{V}_{e,E} \cdot \bar{n}\, dA_e\right) \tag{16}$$

In equations (15) and (16) ρ_e is the density of the exhaust, $\bar{V}_e$ the inertial velocity of the exhaust, $\bar{V}_{e,E}$ the velocity of the exhaust relative to a point fixed on the engine, $\bar{V}_{e,cg}$ the velocity of the exhaust relative to the vehicle center of gravity, $\bar{r}$ the vector measured from the vehicle center of gravity to the exit face of the nozzle, A_e the exit face area, and $\bar{n}$ a unit vector normal to the exit face. The vectors required in equations (15) and (16) are

$$\bar{V}_e = \bar{i}\left(V_X - V_{e,n} \cos\delta + x_e \dot{\delta} \sin\delta\right) + \bar{j}\left[V_Y + V_{e,n} \sin\delta - \dot{\theta}\left(x_{cg} + x_e \cos\delta\right) + x_e \dot{\delta} \cos\delta\right] \tag{17}$$

$$\bar{V}_{e,E} = -\bar{i} V_{e,n} \cos\delta + \bar{j} V_{e,n} \sin\delta \tag{18}$$

$$\bar{V}_{e,cg} = \bar{i}\left(-V_{e,n} \cos\delta - \dot{x}_{cg} + x_e \dot{\delta} \sin\delta\right) + \bar{j}\left[V_{e,n} \sin\delta - \dot{\theta}\left(x_{cg} + x_e \cos\delta\right) + x_e \dot{\delta} \cos\delta\right] \tag{19}$$

$$\bar{r} = -\bar{i}\left(x_{cg} + x_e \cos \delta\right) + \bar{j} x_e \sin \delta \tag{20}$$

$$\bar{n} = -\bar{i} \cos \delta + \bar{j} \sin \delta \tag{21}$$

In equations (17), (18), and (19), $V_{e,n}$ is the magnitude of the exhaust gas velocity relative to the nozzle.

Gravity forces.- The gravity forces acting in the axial and lateral directions, respectively, are

$$F_{g,X} = -mg \cos \theta \tag{22}$$

$$F_{g,Y} = mg \sin \theta \tag{23}$$

Differential Equations of Motion

Upon substitution of the kinetic energy from equation (2) and the external forces and moments from equations (4), (5), and (6) into equations (1), the following set of differential equations is obtained to describe the vehicle motions:

$$\dot{V}_X - \dot{\theta} V_Y = \frac{F}{m} - g(\cos \theta) - \frac{qA_o}{m} C_X \tag{24}$$

$$\dot{V}_Y + \dot{\theta} V_X = -\frac{F}{m} \delta + g(\sin \theta) + \frac{\dot{m}}{m}\left(-x_{cg}\dot{\theta} + x_e\dot{\delta}\right) + \frac{qA_o}{m} C_{N_\alpha}\left(\alpha + \alpha_w\right) + \frac{qA_o l_B}{mV} C_{N_{\dot{\theta}}}\dot{\theta} \tag{25}$$

$$\ddot{\theta} = \left[\frac{F}{I}\left(x_{cg} - x_e\right) + \frac{S_E \dot{V}_X}{I}\right]\delta - \frac{\dot{I}}{I}\dot{\theta} + \frac{\dot{m}}{I}\left(x_{cg}{}^2\dot{\theta} - x_e x_{cg}\dot{\delta}\right) + \frac{qA_o l_B}{I} C_{m_\alpha}\left(\alpha + \alpha_w\right) + \frac{qA_o l_B{}^2}{IV} C_{m_{\dot{\theta}}}\dot{\theta} \tag{26}$$

where

$$F = \rho_e A_e V_{e,n}{}^2 \tag{27}$$

The following equations were utilized in the solution of equations (24), (25), and (26):

$$\alpha = \tan^{-1} \frac{-V_Y}{V_X} \tag{28}$$

$$\gamma = \theta - \alpha \tag{29}$$

$$h = h_o + \int_{t_o}^{t} V_i \cos \gamma \, dt \tag{30}$$

The vehicle is assumed to be flying a vertical trajectory with constant thrust and to be losing mass at a constant rate according to the relation

$$m = m_o + \mu t \tag{31}$$

where

$$\mu = -\rho_e A_e V_{e,n} \tag{32}$$

Control is maintained by rotating the thrust vector according to the first-order differential equation

$$\tau\dot{\delta} + \delta = \delta_c \tag{33}$$

with δ_c, the command to the thrust vector, provided by a simple autopilot. The quantities used to steer the vehicle are attitude and attitude rate, as given by the relation

$$\delta_c = -\left(\beta K_1 \theta + \Gamma K_2 \dot{\theta}\right) \tag{34}$$

where K_1 and K_2 are the nominal attitude and attitude-rate gains, respectively, and β and Γ are multiplicative constants.

In obtaining the differential equations of motion (eqs. (24), (25), (26), and (33)), the following simplifications were made:

1. The thrust-vector rotation angle was assumed to be small, and thus $\sin \delta = \delta$ and $\cos \delta = 1$.

2. The aerodynamic effects associated with pitching acceleration and rate of change of angle of attack were neglected.

3. The rate of travel of the vehicle's center of gravity within the vehicle was small and thus was neglected.

The coefficients of the equations of motion, equations (24), (25), and (26), vary with time since the mass, center-of-gravity location, moment of inertia, and atmospheric density all change during the flight. The equations were programed and solved on an analog computer. All computer runs were started at an altitude of 5,000 feet in order to reduce machine time. The proper initial conditions were obtained from a computer run for a no-wind vertical ascent. The nonzero initial conditions at $t = 31$ seconds are $h_o = 5{,}000$ feet and $V_X = 274.37$ ft/sec.

CONFIGURATION

Vehicle

The launch-vehicle configurations assumed for this study are shown in figure 2. The characteristics of the launch vehicle are as follows:

Thrust, F, lb	12×10^6
Specific impulse, I_{sp}, sec	260
Length, l_B, ft	352
Initial mass, m_o, lb-sec^2/ft	0.289×10^6
Rate of mass loss, μ, lb-sec/ft	-1,433.3
Base area, A_o, sq ft	1,520
Engine static unbalance, S_E, lb-sec^2	33,534
Thrust-vectoring time lag, τ, sec	0.05

It is a vehicle of the Nova class having 12×10^6 pounds of thrust and weighing 9.3×10^6 pounds at lift-off. Two versions of this vehicle are considered - with and without fins. No allowance was made in the study for the weight or drag of the fins. The fins were selected to reduce by 50 percent the destabilizing pitching-moment coefficient at maximum dynamic pressure. The mass, center-of-gravity location, and moment of inertia of the total vehicle are presented in figure 3. Aerodynamic coefficients are presented in figure 4. The axial-force

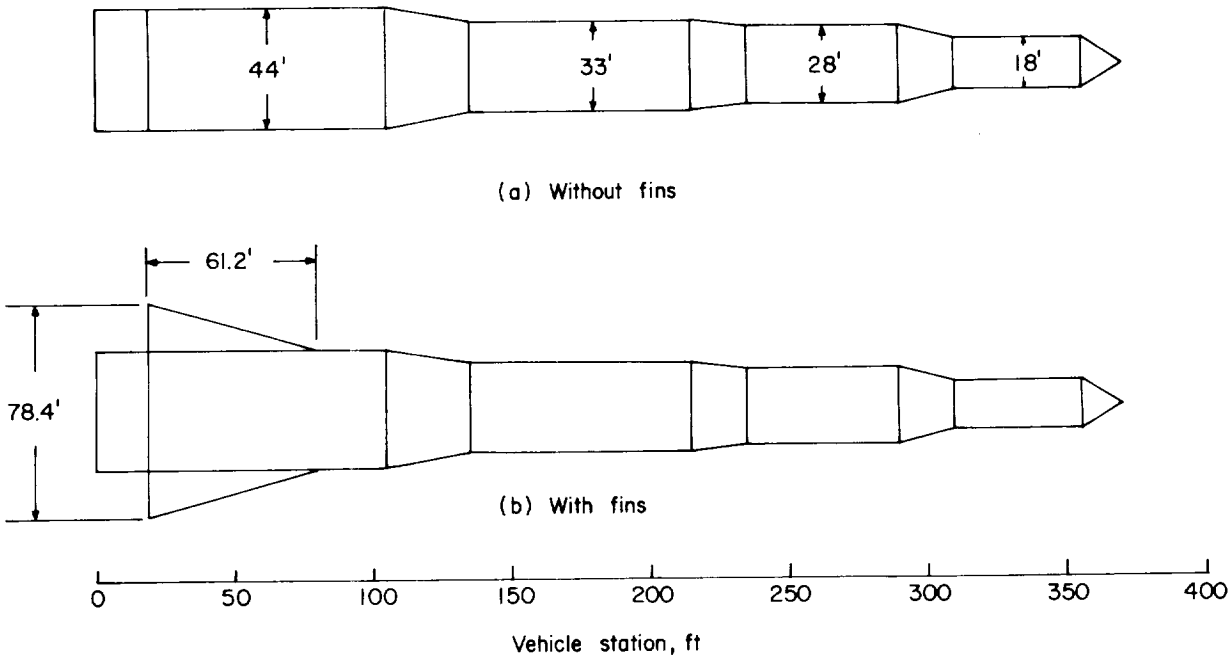

Figure 2.- Launch-vehicle configurations.

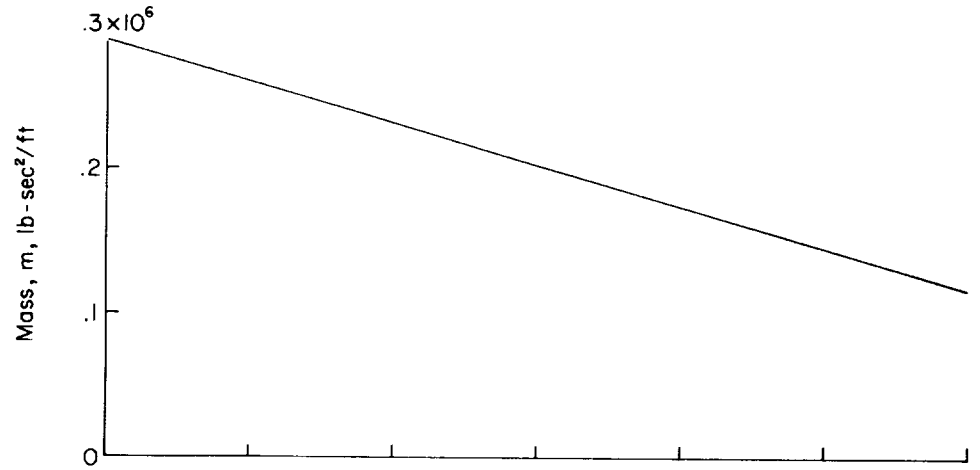

(a) Vehicle mass.

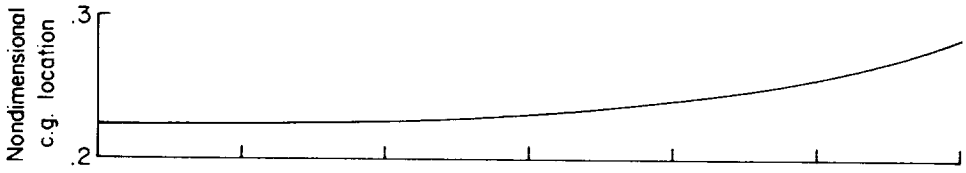

(b) Center-of-gravity location, x_{cg}/l_B.

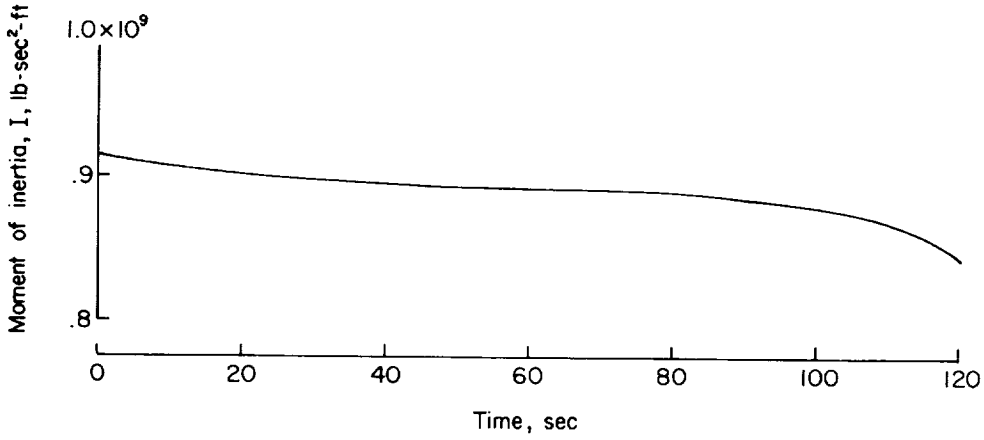

(c) Moment of inertia about the center of gravity.

Figure 3.- Mass properties of the launch vehicle.

coefficient in figure 4(a) is a function of Mach number and was estimated from data for similar configurations. The normal-force and pitching-moment coefficients in figures 4(b) and 4(c) were calculated by using momentum theory as in reference 3. This theory gives expressions for the normal force and pitching moment which are independent of Mach number. The contribution of the fins to the

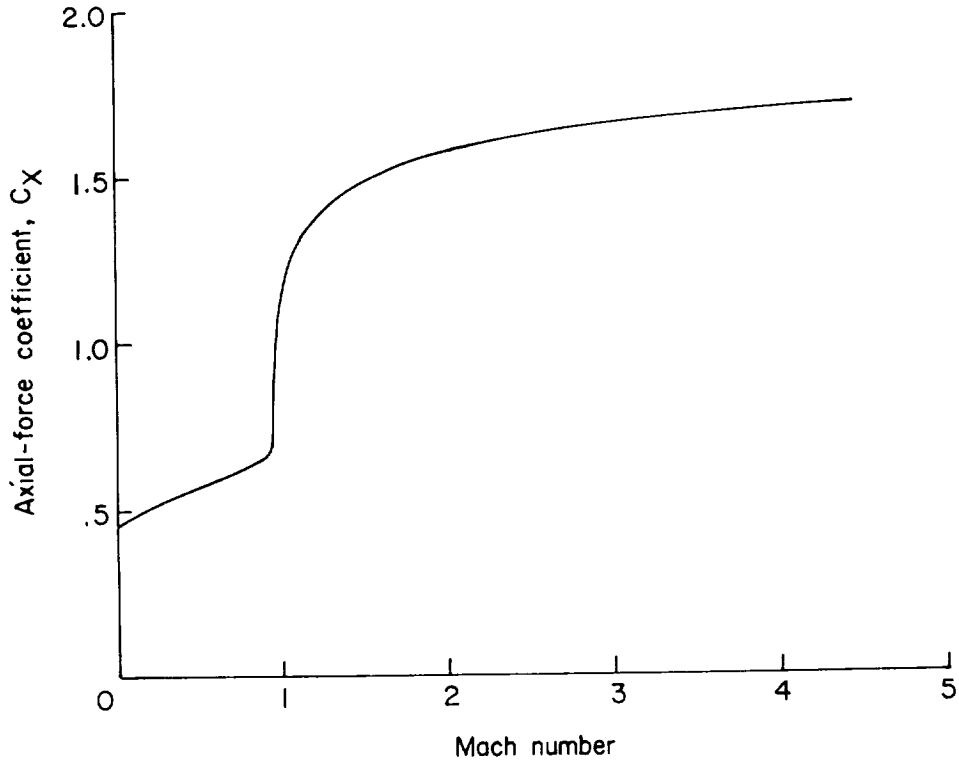

(a) Variation of axial-force coefficient with Mach number.

Figure 4.- Aerodynamic characteristics of the vehicles.

total aerodynamic characteristics of the vehicle was estimated by the method of reference 5. Mach number effects on the fins were neglected since a calculated value of the normal-force-curve slope based on slender-body theory was used.

Control System

The control system employed attitude and attitude-rate feedback to maintain the vertical attitude of the vehicle. Nominal control-system gains were calculated by the method of reference 6 with f_p, the undamped controlled pitch frequency, specified as 0.2 cps and ξ_p, the ratio of damping of the controlled pitch mode to critical damping, specified as 0.75. The resulting control-system gains, presented in figure 5 for the unfinned vehicle, are functions of time because of

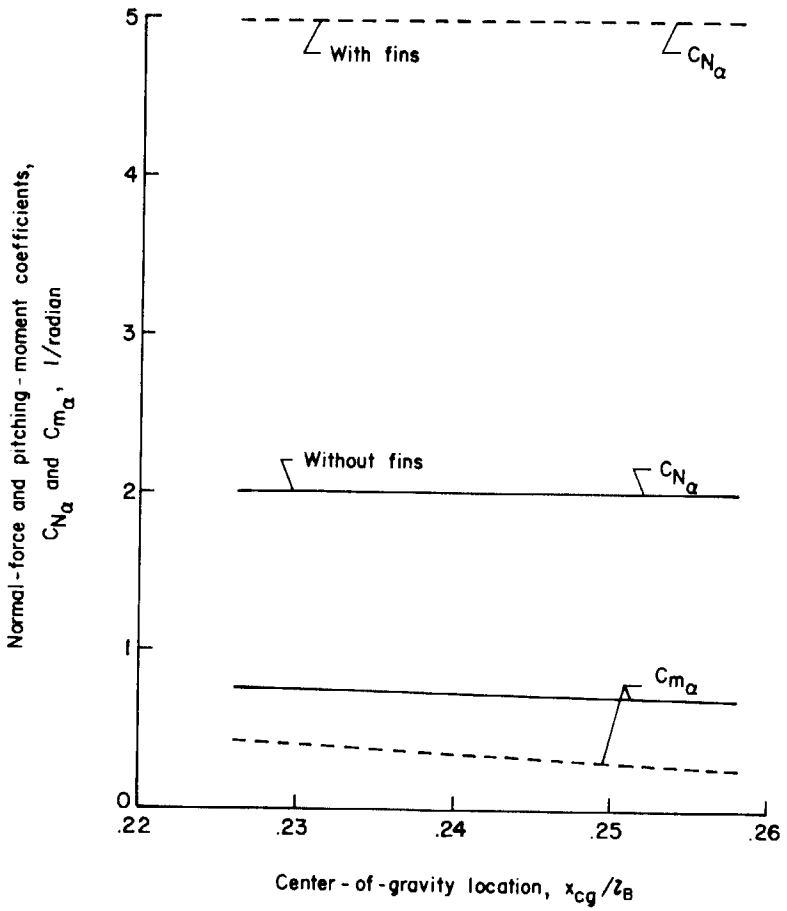

(b) Variation of normal-force and pitching-moment coefficients with center-of-gravity location.

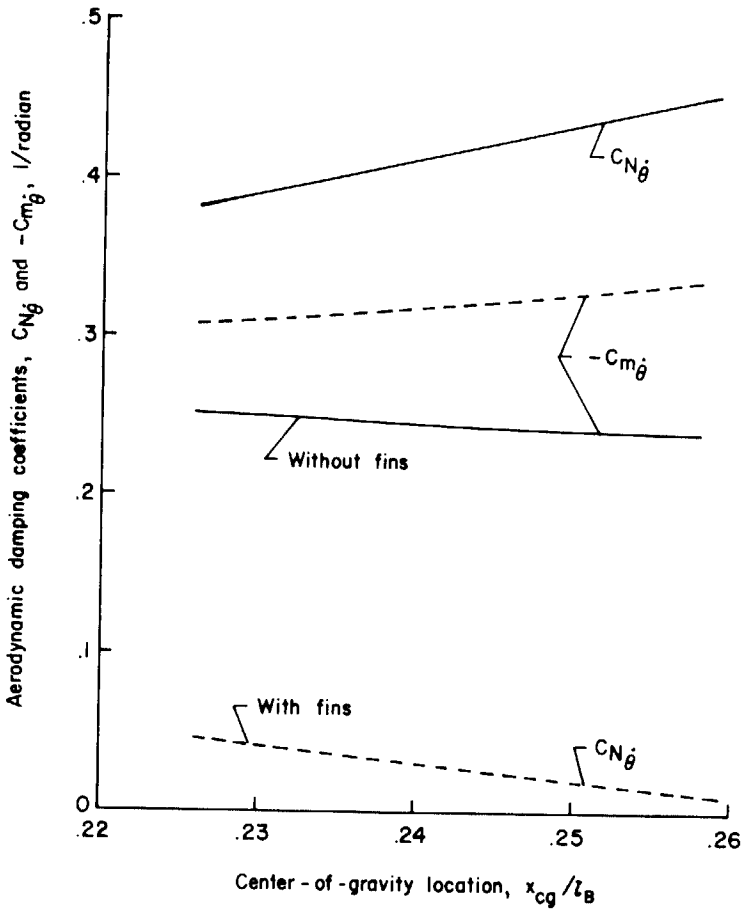

(c) Variation of aerodynamic damping coefficients with center-of-gravity location.

Figure 4.- Concluded.

WIND PROFILES

The wind profiles used in the study were based on reference 1 and are shown in figure 7. These are wind profiles synthesized from a large statistical sample of balloon-measured winds. Two wind profiles were considered - one with a maximum wind speed of 300 ft/sec that will be exceeded only 1 percent of the time and one with a maximum wind speed of 256 ft/sec which will be exceeded 5 percent of the time. The peak wind speed on these synthetic profiles occurs at an altitude of 35,000 feet near the point of maximum dynamic pressure, where aerodynamic forces are greatest.

RESULTS AND DISCUSSION

Linear System

The two vehicles, finned and unfinned, were first flown through the 1- and 5-percent wind profiles with no limit (or stops) on the thrust-vector rotation

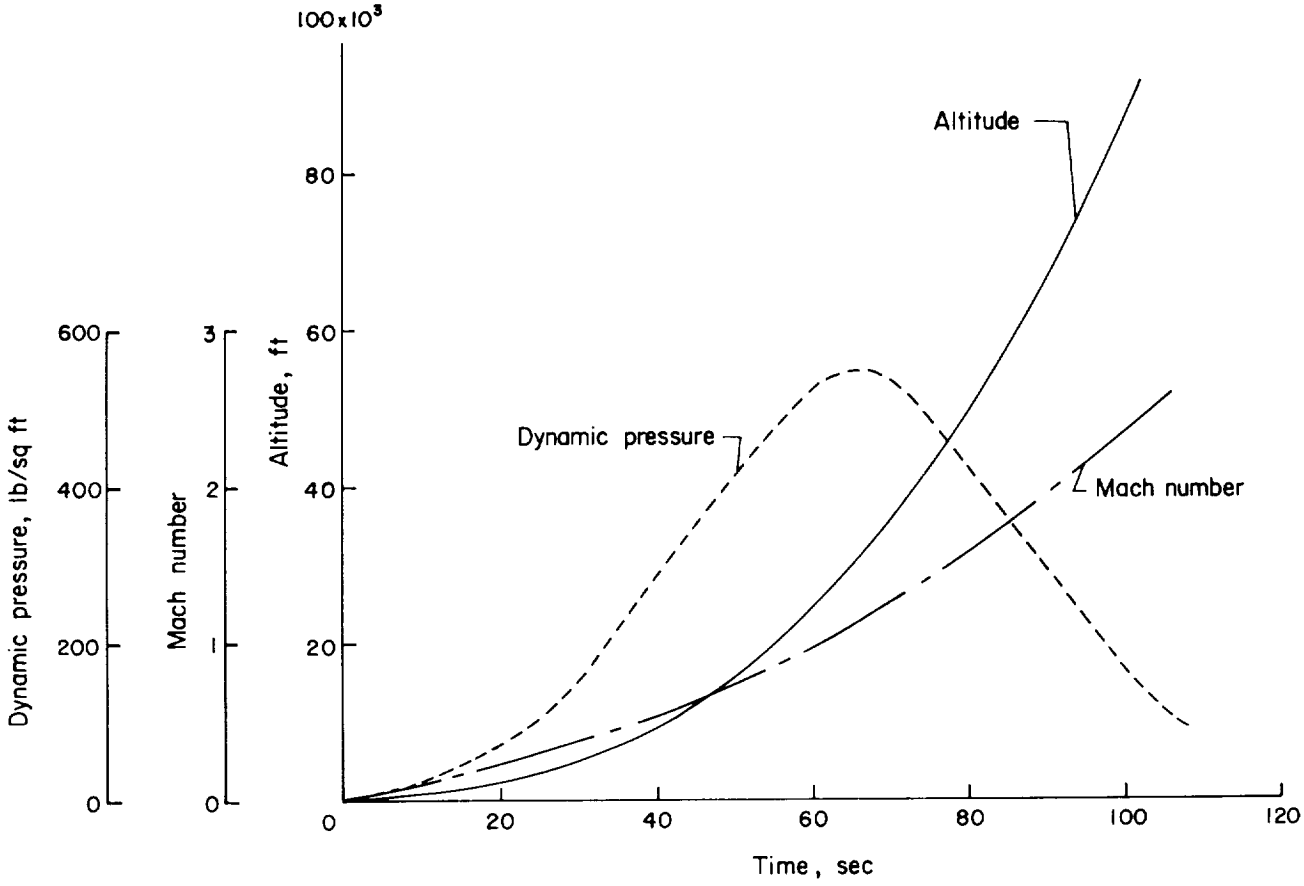

Figure 6.- Altitude, Mach number, and dynamic-pressure variation with time for vertical ascent with no wind.

the varying mass and aerodynamic properties of the vehicle. Variations in gain about the nominal values were made by multiplying these curves by constants. The

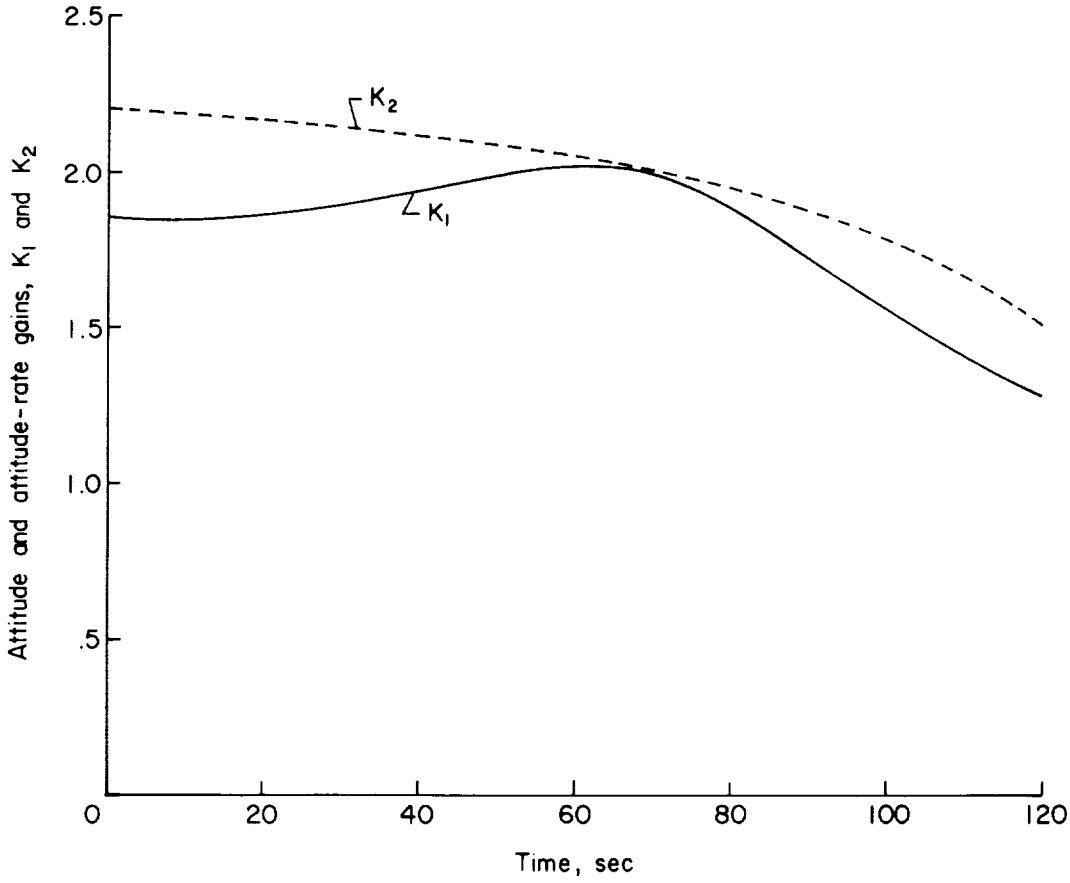

Figure 5.- Nominal attitude and attitude-rate gains.

trajectory parameters required to predict the aerodynamic forces used in determining the gains were based on the vertical ascent of an ideal rocket with no drag, a thrust-weight ratio at lift-off that matches the present configuration, and a specific impulse of 260 seconds.

TRAJECTORY

A no-wind trajectory for the vehicle was computed for use in determining initial conditions and is shown in figure 6. Altitude, dynamic pressure, and Mach number are shown as functions of time for the vertical ascent. The 1959 ARDC standard atmosphere was used (ref. 7). The maximum dynamic pressure of 550 lb/sq ft occurs 66 seconds after lift-off at an altitude of 31,000 feet and a Mach number of 1.15.

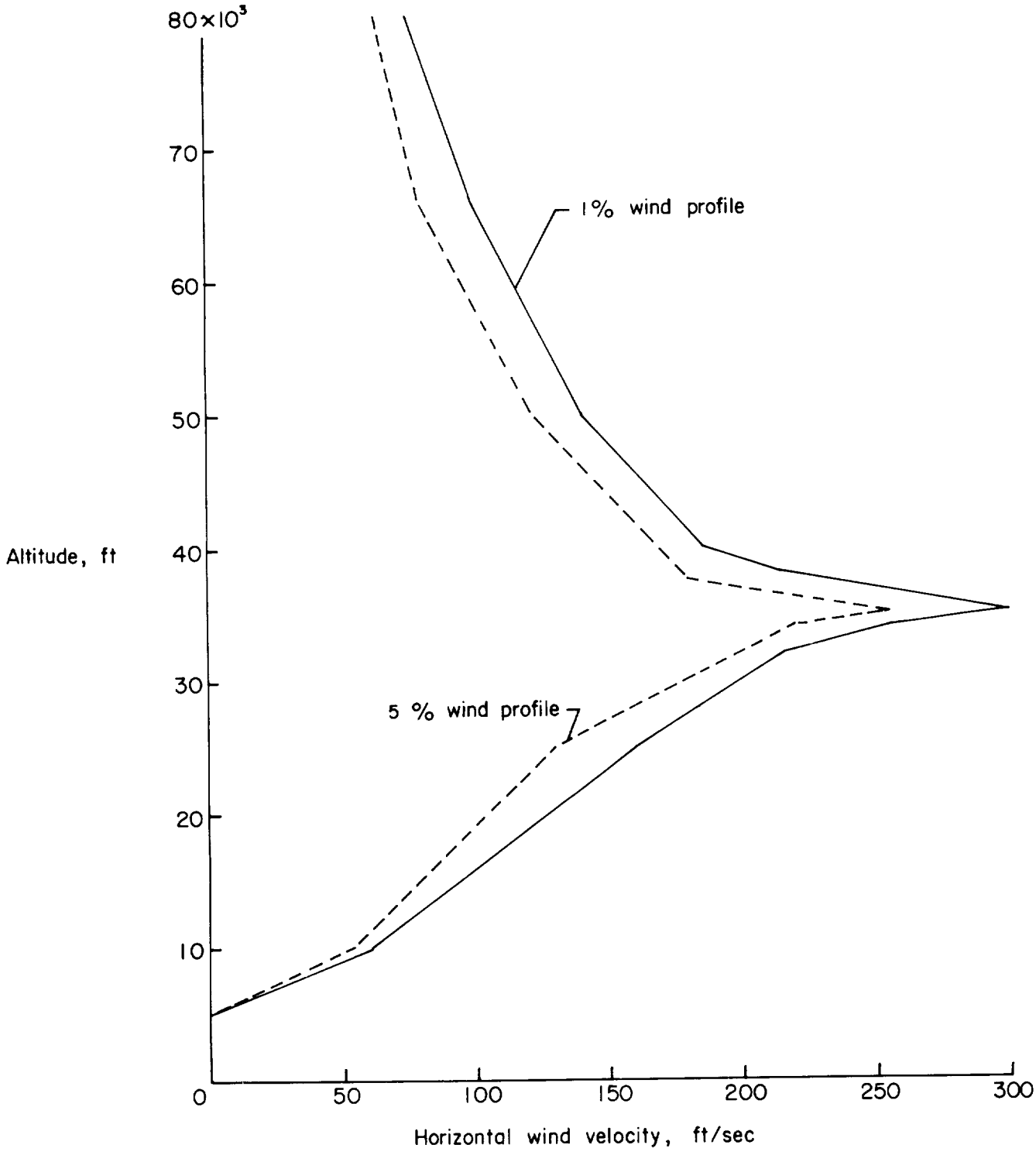

Figure 7.- Synthetic wind profiles.

angle. With no limit on this angle, the system will be referred to as linear. These runs were made to establish the thrust-vector-angle requirements and the attitude-angle deviations for various values of the gain multipliers β and Γ.

Time histories.- Time histories of the response of the unfinned vehicle with nominal gain values are shown in figure 8. Responses of the finned vehicle are similar to those of the unfinned vehicle, though magnitudes are generally smaller. The input wind for this case, the 1-percent profile, is shown as a function of time in figure 8(a). The angle of attack, in figure 8(b), reaches a peak value of about 10.3° and coincides in time with the peak wind velocity. The thrust-vector angle (fig. 8(c)) has a maximum value of about -3°. The attitude angle (the angular deviation of the body axis from the vertical) is illustrated in figure 8(d). The maximum value of about 1.3° lags behind the maximum wind by about

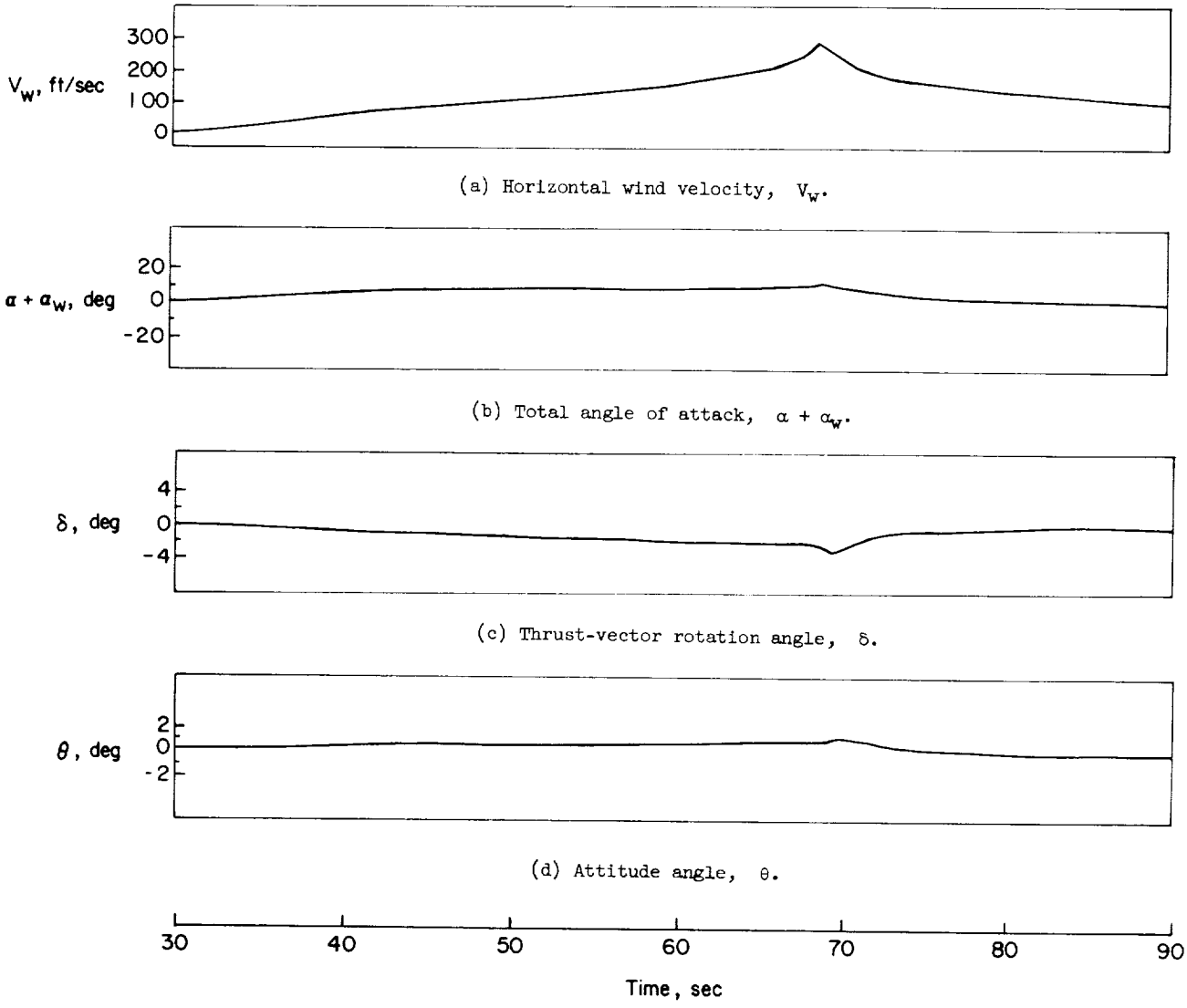

Figure 8.- Time histories of flight through the 1-percent wind profile with nominal gain values and unlimited thrust-vector rotation angle.

a second because of the large inertia of the vehicle. Note that an attitude error gradually builds up after lift-off as a result of the increasing wind velocity. A more sophisticated control system might have reduced this error.

Thrust-vector rotation-angle requirements.- The thrust-vector rotation angles required to fly the vehicles through the two wind profiles are shown in figure 9. In figure 9(a) the maximum thrust-vector angle is shown as a function of the ratio of attitude gain to nominal attitude gain, with nominal rate gain. For the range investigated, increasing the attitude gain caused only a slight increase in the required thrust-vector angle. Note that the finned vehicle requires less than half the thrust vectoring that is required by the unfinned vehicle. This reduction in required angle corresponds approximately to the reduction in destabilizing aerodynamic moment caused by the addition of fins to the vehicle. The finned vehicle also requires only about a 15-percent larger thrust-vector angle to fly through the 1-percent wind than the 5-percent wind, whereas the unfinned vehicle requires about a 25-percent larger thrust-vector angle.

Figure 9(b) shows the maximum required thrust-vector angle as a function of the ratio of rate gain to nominal rate gain, with the attitude gain held constant at the nominal value. For the range of rate gains studied, the required thrust-vector angle is constant. The differences in required thrust-vector angle between

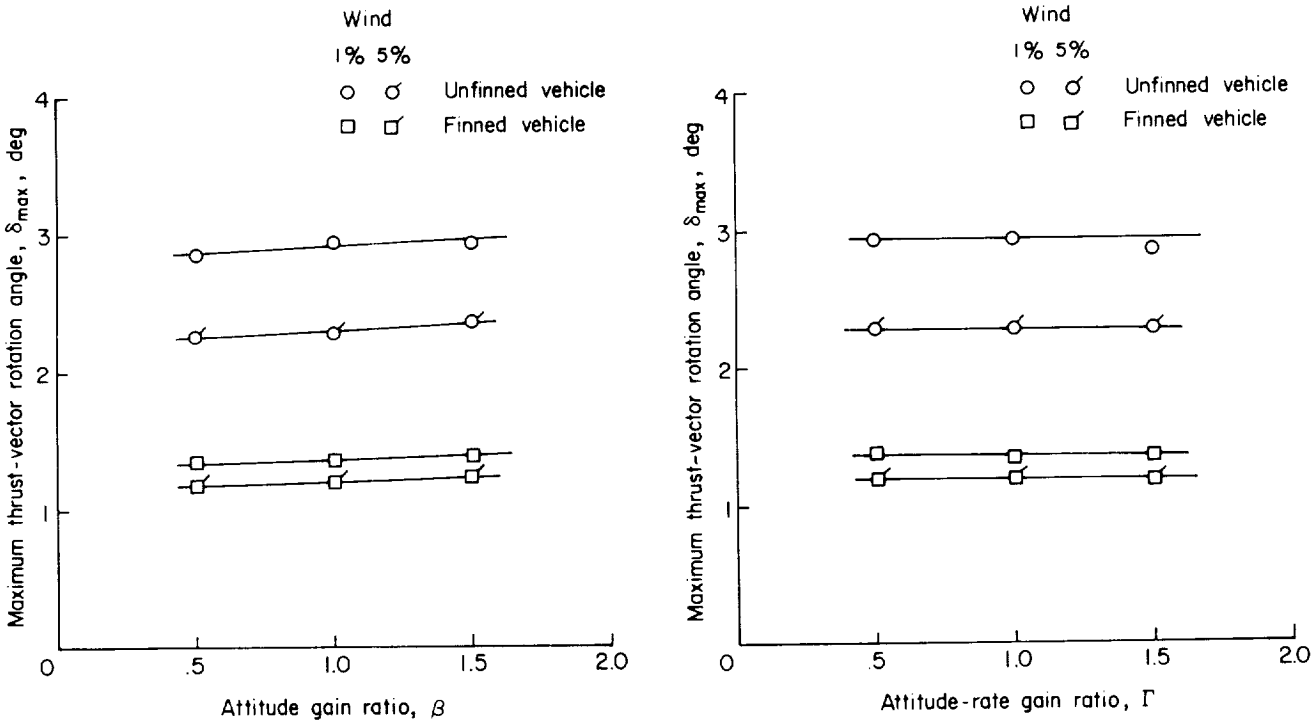

(a) Required thrust-vector angle as a function of attitude gain with nominal rate gain.

(b) Required thrust-vector angle as a function of rate gain with nominal attitude gain.

Figure 9.- Engine thrust-vector rotation-angle requirements for linear operation.

the finned and unfinned vehicles and between the two input wind profiles are the same as in figure 9(a).

Maximum attitude-angle deviations.- The maximum thrust-vector rotation angle required by a particular vehicle to fly through a particular wind profile has been shown by figure 9 to remain nearly constant for a wide range of control gains. However, the maximum attitude deviation from the vertical reference does vary considerably as gains are changed, as illustrated by figure 10. The maximum attitude angle is shown as a function of the ratio of attitude gain to nominal attitude gain for flight through the 1-percent wind profile. Curves are shown for both the finned and the unfinned vehicle and for three ratios of rate gain to nominal rate gain. Increasing the attitude gain decreases the maximum attitude angle, as would be expected for a "tighter" control system. In all cases, maximum attitude angles for the unfinned vehicle are about twice those for the finned vehicle. However, changes in rate gain are seen to cause only minor changes in the maximum attitude angle.

Temporarily Unstable System

The finned and unfinned vehicles were flown through the 1- and 5-percent wind profiles with the thrust-vector angle limited at several different values. The system gains were varied as in the linear case.

Time histories.- Typical time histories of the response of the unfinned vehicle with nominal gains and a limited thrust-vector angle are presented in figure 11. Again the input wind is the 1-percent profile shown in figure 7 as a function of altitude and in figure 11(a) as a function of time. The angle of attack (fig. 11(b)) has a maximum value of 10.3° occurring at the same time as the maximum wind velocity. The thrust-vector angle (fig. 11(c)) has a maximum limited value of -2.25° for a period of 5.6 seconds. The attitude angle (fig. 11(d)) has a maximum value of 2.75° but lags behind the maximum wind velocity by approximately 2 seconds because of the large inertia of the vehicle. The temporarily unstable condition is illustrated by these time histories. At the instant that the thrust-vector angle reaches its limit, the attitude angle θ begins to diverge. However, the

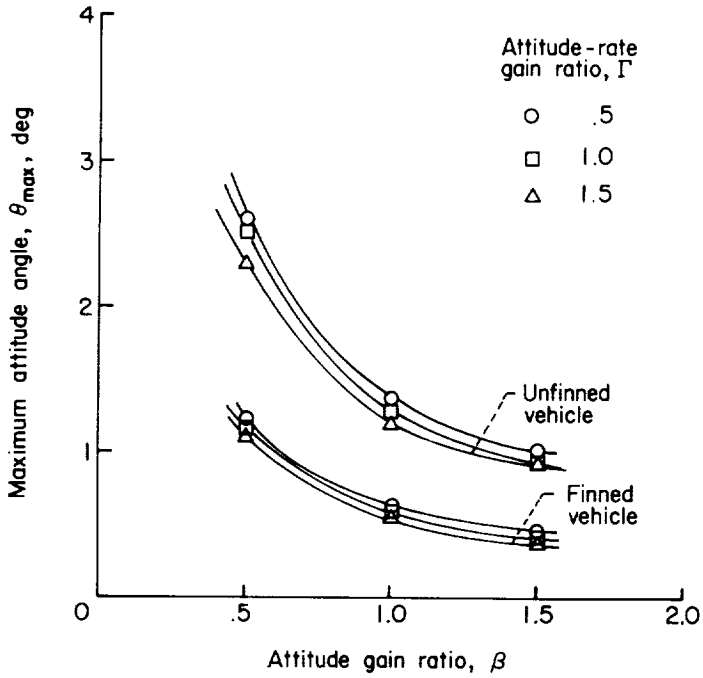

Figure 10.- Maximum attitude angle of the linear system as a function of control-system gains for flight through the 1-percent wind profile.

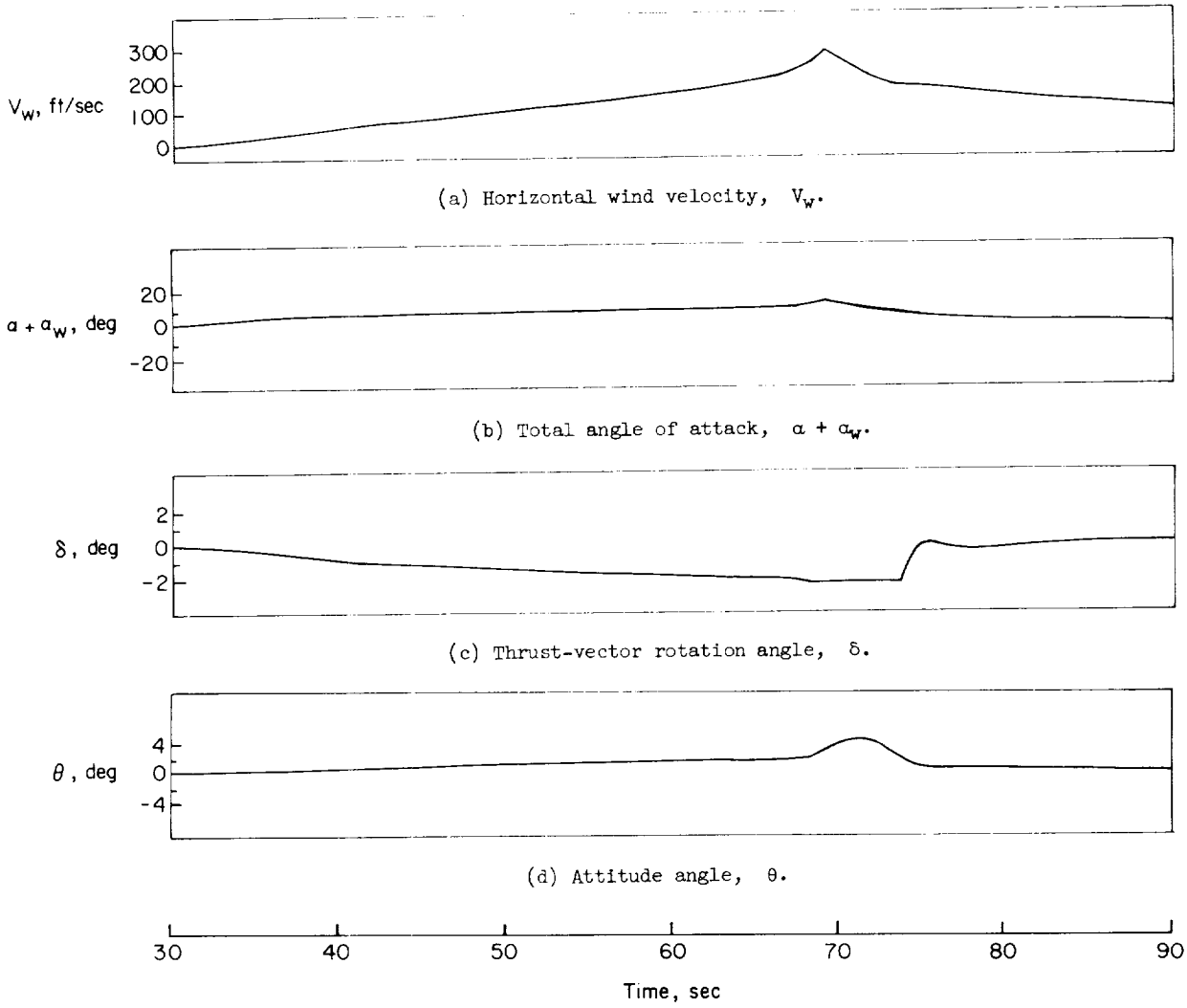

Figure 11.- Time histories of flight through the 1-percent wind profile with nominal gain values and the thrust-vector rotation angle limited to $2\frac{1}{4}^{\circ}$.

rate of divergence decreases when the wind shear reverses. When the restoring moment due to the thrust vector again exceeds the upsetting moment, the thrust-vector rotation angle recedes from the limit and the system behaves in a linear fashion. In addition to the wind shear reversal, control recovery at this time is aided by decreasing dynamic pressure. Thus, control of the vehicle after a temporary unstable condition is demonstrated.

Attitude variation.- The attitude variation as a function of limit thrust-vector angle is shown in figure 12 for both the finned and unfinned vehicles. The control system had nominal gains and the vehicles were flown through 1- and 5-percent winds. Again the unfinned vehicle demonstrates the greater maximum attitude variation. The curves are constants at limit thrust-vector angles above

the angle required by the linear system. At lower values of the limit thrust-vector angle the system is unstable because the upsetting moment is greater than the restoring moment. As the limit thrust-vector angle is reduced below the value required by the linear system, the system is capable of recovery as illustrated in figure 11, but increasingly large attitude angles occur. In each case studied, there was a limit thrust-vector angle below which the system diverged and recovery was not possible. These minimum limit thrust-vector angles were not determined exactly but are known to within $1/4^{\circ}$ since they lie somewhere between the last two points on the curves of figure 12. It should be noted, however, that there is a range of limit thrust-vector angles in which a temporarily unstable condition can be tolerated since control is recovered after the vehicle passes through the wind shear reversal.

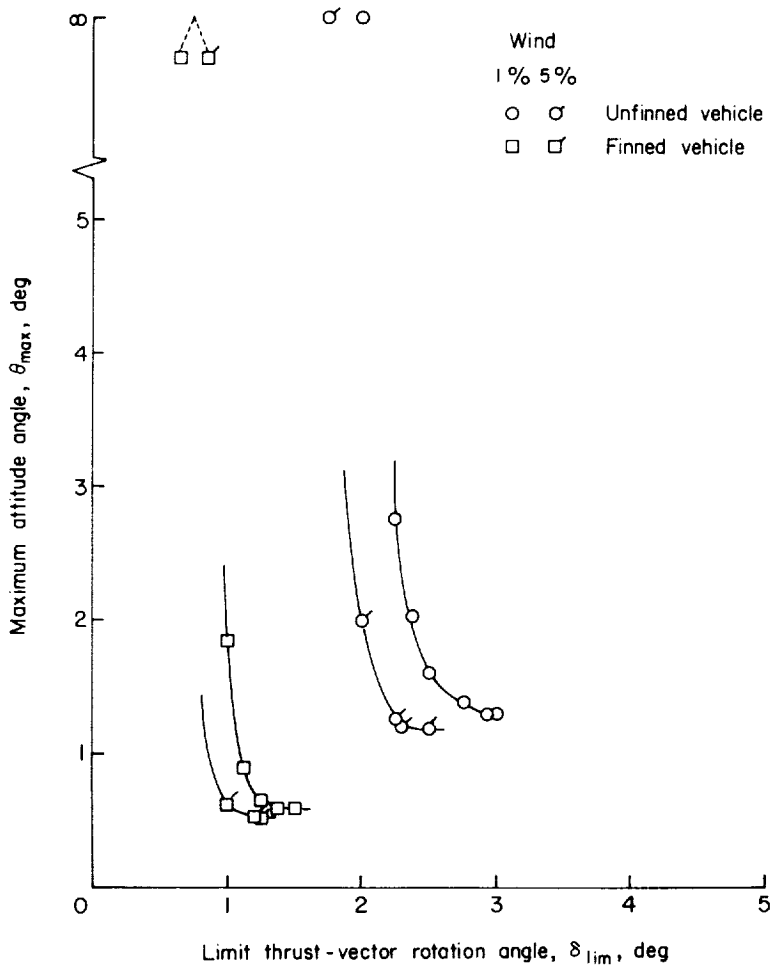

Figure 12.- Variation of maximum attitude angle with limit thrust-vector rotation angle for nominal gains.

Effects of attitude and attitude-rate gains on the attitude variation with limit thrust-vector angle are shown in figures 13(a) and 13(b), respectively, for both the finned and unfinned vehicles flying through the 1-percent wind profile. In figure 13(a) the rate gain is held constant at the calculated nominal value and the attitude gain takes on values of 50 percent, 100 percent, and 150 percent of the calculated nominal value. In figure 13(b) the attitude gain is held constant at the calculated nominal value and the rate gain takes on values of 50 percent, 100 percent, and 150 percent of the calculated nominal value. The higher values of gain ($\beta = 1.5$ and $\Gamma = 1.5$) represent a relatively tight control system and the low values ($\beta = 0.5$ and $\Gamma = 0.5$) a relatively loose control system. The curves in figures 13(a) and 13(b) indicate that the vehicles are much more sensitive to changes in attitude gain than to changes in rate gain. The tighter control systems allow much less attitude variation than do the loose ones for a given limit thrust-vector angle. However, the minimum value of the limit thrust-vector angle at which recovery is possible is essentially independent of the gain values. Thus, for a given vehicle flying through

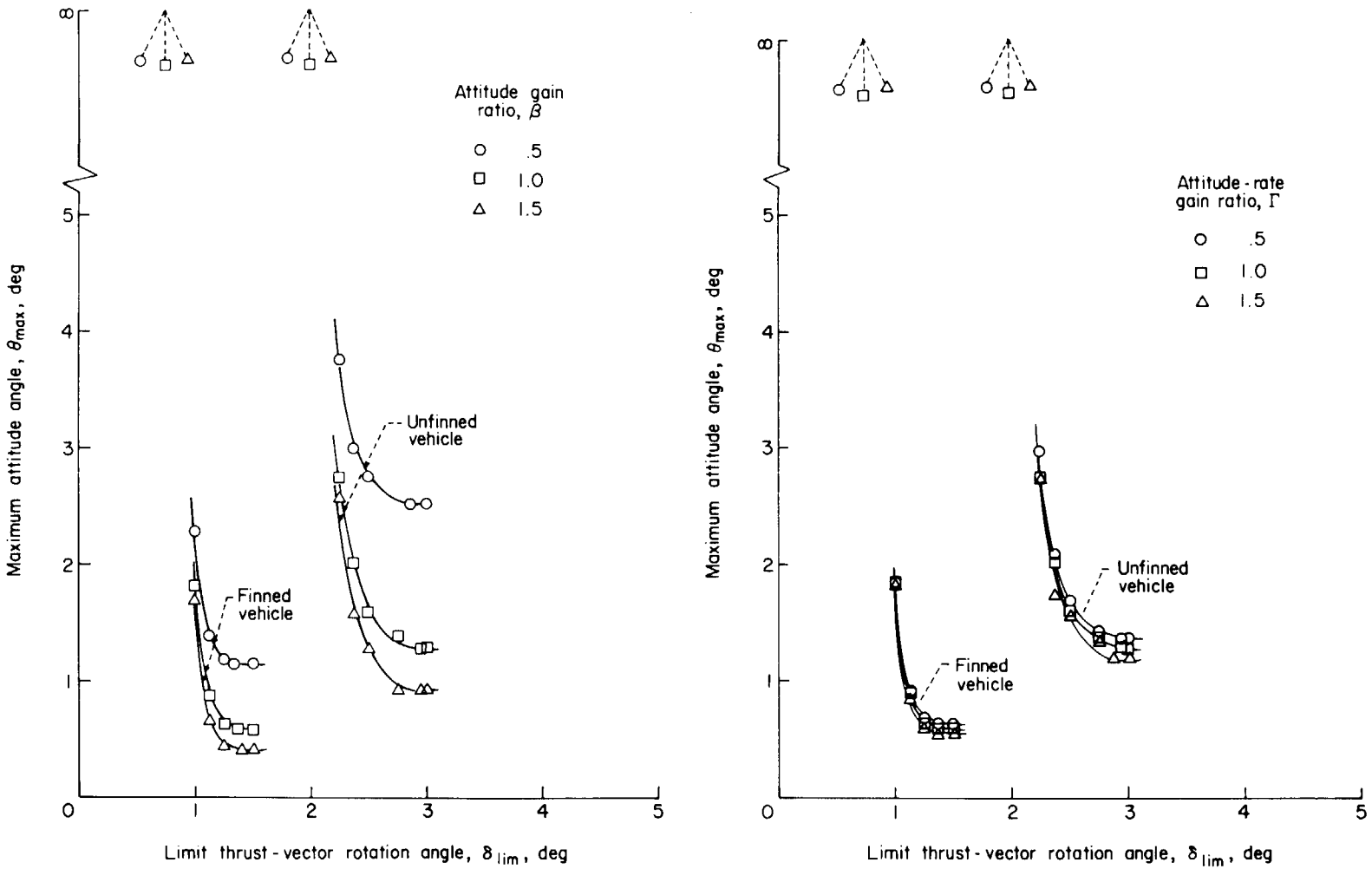

(a) With nominal rate gain.

(b) With nominal attitude gain.

Figure 13.- Maximum attitude angle as a function of limit thrust-vector rotation angle for the 1-percent wind profile.

a given wind profile, there is some minimum value of limit thrust-vector angle, independent of the control system, below which the vehicle will diverge.

Figure 14 shows the variation of maximum attitude angle with the time that the thrust-vector angle is held in the limited position while the vehicle traverses the 1-percent profile. This time is the period the vehicle is unstable. These curves are plotted for the nominal rate gain and several values of attitude gain. The maximum attitude-angle deviation increases as the limit time increases. The large limit times correspond to small values of the limit thrust-vector rotation angle. Again the effect of control-system tightness is evident from the three curves for different attitude gains, with the tighter control ($\beta = 1.5$ and $\Gamma = 1.5$) allowing the smallest attitude variation. This figure indicates that control could be regained after periods of instability as long as 5 or 6 seconds.

Angle-of-attack variations.- Figure 15 shows time histories of angle of attack for several limit thrust-vector angles for the unfinned vehicle with nominal gains flying through the 1-percent wind profile. The limit thrust-vector angle decreases from $2\frac{3}{4}^{\circ}$ in figure 15(b) to $2\frac{1}{8}^{\circ}$ in figure 15(d). Notice that the maximum angle of attack is almost constant in all cases even though the attitude variation has been shown to increase markedly with decreasing limit thrust-vector angle (fig. 13). The maximum angle of attack is seen to occur at the peak of the wind speed. This almost constant maximum angle of attack is a result of the long response time of the vehicle due to the large inertia in pitch. The vehicle passes the point of maximum wind before it has time to respond to the wind spike. This result is most evident in figure 15(d), where the angle of attack due to body motion prevents the rapid decay of the total angle of attack exhibited in figures 15(b) and 15(c). Thus, the maximum total angle of attack is determined by the maximum wind velocity alone for cases in which the vehicle is controllable.

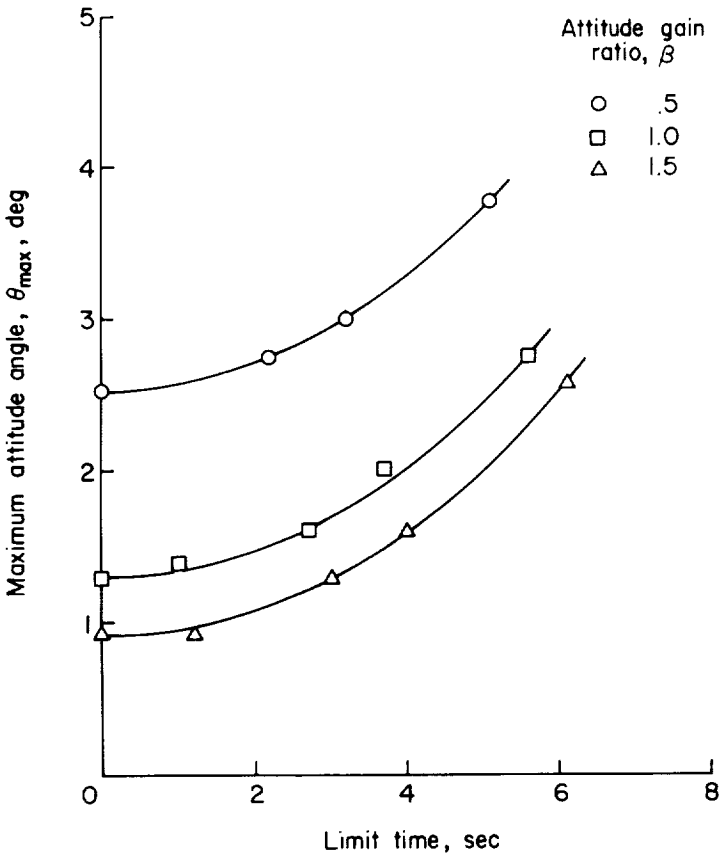

Figure 14.- Maximum attitude angle as a function of the time that the thrust-vector rotation angle is limited. Nominal rate gain and 1-percent wind-profile input.

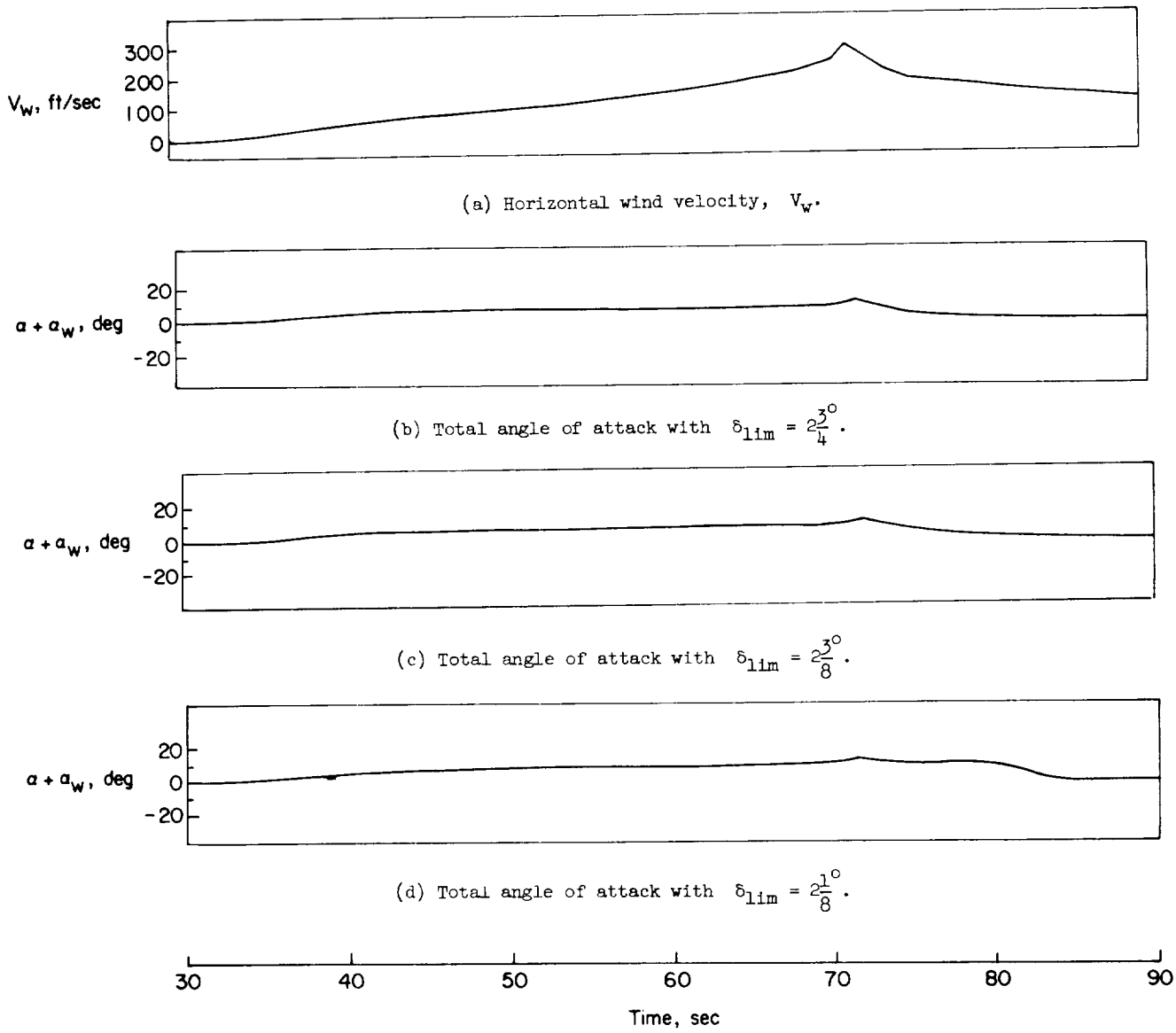

Figure 15.- Time histories of angle of attack for decreasing limit thrust-vector rotation angles for flight of the unfinned vehicle through the 1-percent wind profile.

CONCLUDING REMARKS

The ability of a large launch vehicle to negotiate safely large atmospheric wind disturbances while in a temporarily unstable state due to limited thrust vectoring has been investigated. The results indicate that, in some cases, vehicle control can be reestablished after temporary divergence while passing through the wind disturbance. However, there is a minimum value of the limit thrust-vector angle, independent of gain, below which the vehicle is divergent. In most cases in which control recovery was possible, the maximum angle of attack was dependent only on the maximum wind velocity.

These results indicate that a launch vehicle might be utilized for a particular mission even though mission requirements, such as launching in high winds

or using alternate payload shapes, indicate a need for increased thrust-vector-angle capability. These results can also be interpreted to indicate that a control system which has been designed with adequate thrust vectoring to maintain control for specified wind and payload conditions has an additional safety factor in its ability to recover from temporary instabilities.

Langley Research Center,
National Aeronautics and Space Administration,
Langley Station, Hampton, Va., June 10, 1963.

REFERENCES

1. Sissenwine, Norman: Windspeed Profile, Windshear, and Gusts for Design of Guidance Systems for Vertical Rising Air Vehicles. Air Force Surveys in Geophysics No. 57 (AFCRC-TN-54-22), Air Force Cambridge Res. Center, Nov. 1954.

2. Thomson, William Tyrrell: Introduction to Space Dynamics. John Wiley & Sons, Inc., c.1961.

3. Miles, J. W., and Young, Dana: Generalized Missile Dynamics Analysis. III - Aerodynamics. GM-TR-0165-00360, Space Tech. Labs., The Ramo-Wooldridge Corp., Apr. 7, 1958.

4. Housner, George W., and Hudson, Donald E.: Applied Mechanics Dynamics. D. Van Nostrand Co., Inc., c.1950.

5. Pitts, William C., Nielsen, Jack N., and Kaattari, George E.: Lift and Center of Pressure of Wing-Body-Tail Combinations at Subsonic, Transonic, and Supersonic Speeds. NACA Rep. 1307, 1957.

6. Geissler, Ernst D.: Problems in Attitude Stabilization of Large Guided Missiles. Aerospace Eng., vol. 19, no. 10, Oct. 1960, pp. 24-29, 68-71.

7. Minzner, R. A., Champion, K. S. W., and Pond, H. L.: The ARDC Model Atmosphere, 1959. Air Force Surveys in Geophysics No. 115 (AFCRC-TR-59-267), Air Force Cambridge Res. Center, Aug. 1959.